Published in final edited form as:
Ophthalmology. 2009 December ; 116(12): 2305–2314.e2. doi:10.1016/j.ophtha.2009.05.025.

Detection of Macular Ganglion Cell Loss in Glaucoma by Fourier-Domain Optical Coherence Tomography

Ou Tan, Ph.D.[1], **Vikas Chopra, M.D.**[1], **Ake Tzu-Hui Lu, Ph.D.**[1], **Joel S. Schuman, M.D.**[2], **Hiroshi Ishikawa, M.D.**[2], **Rohit Varma, M.D., M.P.H.**[1], and **David Huang, M.D., Ph.D.**[1]

[1]Doheny Eye Institute and Department of Ophthalmology, Keck School of Medicine, University of Southern California, Los Angeles, CA

[2]Department of Ophthalmology, University of Pittsburgh School of Medicine, Pittsburgh, PA

Abstract

Purpose—To map ganglion cell complex thickness with high-speed Fourier-domain optical coherence tomography (FD-OCT) and compute novel macular parameters for glaucoma diagnosis.

Design—Observational, cross-sectional study.

Participants—One hundred seventy-eight participants in the Advanced Imaging for Glaucoma Study, divided into three groups: 65 persons in the normal group (N), 78 in the perimetric glaucoma group (PG), and 52 in the pre-perimetric glaucoma group (PPG).

Methods—The RTVue FD-OCT system was used to map the macula over a 7×6 mm region. The macular OCT images were exported for automatic segmentation using software we developed. The program measured macular retinal (MR) thickness and ganglion cell complex (GCC) thickness. The GCC was defined as the combination of nerve fiber, ganglion cell, and inner plexiform layers. Pattern analysis was applied to the GCC map and the diagnostic power of pattern-based diagnostic parameters were investigated. Results were compared to time-domain (TD) Stratus OCT measurements of MR and circumpapillary nerve fiber layer (NFL) thickness.

Main Outcome Measures—Repeatability was assessed by intraclass correlation (ICC), pooled standard deviation, and coefficient of variation. Diagnostic power was assessed by the area under the receiver operator characteristic (AROC) curve. Measurements in the PG group were the primary measures of performance.

Results—The FD-OCT measurements of MR and GCC averages had significantly better repeatability than TD-OCT measurements of MR and NFL averages. The FD-OCT GCC average had significantly (P=0.02) higher diagnostic power (AROC = 0.90) than MR (AROC = 0.85 for both FD-OCT & TD-OCT) in differentiating between PG and N. One GCC pattern parameter, global loss volume, had significantly higher AROC (0.92) than the overall average (P=0.01). The diagnostic powers of the best GCC parameters were statistically equal to TD-OCT NFL average.

Correspondence and reprint requests to: Ou Tan, Ph.D., Doheny Eye Institute, DVRC160-C, 1355 San Pablo Street, Los Angeles, CA 90033.

Vikas Chopra and Ake Lu made equal contributions to the manuscript.

This article contains online-only material. The following should appear online-only: table 3, figures 3 and figure 6.

Conclusions—The higher speed and resolution of FD-OCT improved the repeatability of macular imaging compared to standard TD-OCT. Ganglion cell mapping and pattern analysis improved diagnostic power. The improved diagnostic power of macular GCC imaging is on par with, and complementary to, peripapillary NFL imaging. Macular imaging with FD-OCT is a useful method for glaucoma diagnosis and has potential for tracking glaucoma progression.

Keywords

optical coherence tomography; glaucoma; imaging; image processing

Glaucoma is characterized by loss of retinal ganglion cells (RGCs) and their respective axons, which comprise the retinal nerve fiber layer (NFL), on pathologic examination.[1–5] RGC loss cannot be seen on slit-lamp ophthalmic examination. Likewise, NFL bundle defects are difficult to detect on clinical examination, and red-free fundus photography to identify and characterize them is rarely used in clinical practice. Thus, glaucoma is diagnosed based on characteristic optic nerve cupping with corresponding visual field deficits. However, since a significant loss to RGC population can occur prior to detectable visual field deficits and that structural loss can precede detectable function loss by up to 5 years,[6–9] developing methods to quantify RGC-related glaucomatous changes could lead to glaucoma detection at an earlier stage and more accurate tracking of glaucoma progression.

A significant proportion of RGC population resides in the macula but is clinically undetectable on ophthalmoscopic examination. Reduced macular thickness in glaucoma was initially described by Zeimer et al using the slit-scanning Retinal Thickness Analyzer[10] (RTA, Talia Technology Ltd., Neve-Ilan, Israel). Since the introduction of optical coherence tomography (OCT) by Huang et al,[11] it has proven useful for measuring circumpapillary nerve fiber layer thickness (NFL) for glaucoma detection. However, total macular retinal (MR) thickness measurement using OCT has not been nearly as accurate a diagnostic parameter as NFL.[12–14]

Two recent studies from our group found that glaucoma diagnostic accuracy could be improved if macular measurements by OCT are focused on the inner retinal layers[15, 16], Glaucoma preferentially affects the three innermost retinal layers: the nerve fiber, ganglion cell, and inner plexiform layers, which contain, respectively, the axons, cell bodies, and dendrites of the ganglion cells. Therefore, we refer to the combination of these three layers as the ganglion cell complex (GCC) (Fig. 1).

In this study, we investigate the diagnostic potential of macular ganglion cell complex (GCC) thickness mapping and analysis using a newer Fourier-domain (FD) OCT[17–20] system (also called spectral or spectral domain OCT[21–27]). The FD-OCT system has higher resolution and speed compared to the time-domain (TD) OCT system we previously studied. The higher speed enables mapping of the macula over a wider area with many more sampling points. The higher resolution facilitates delineation of GCC from the rest of retina. The potential for improved repeatability and diagnostic power was assessed in a cross-sectional clinical study.

Method

Clinical Study

Participants in the prospective, longitudinal Advanced Imaging for Glaucoma Study (AIGS) between the periods of 2003 and 2007 were included. The earliest available FD-OCT scans for each participant, along with the TD-OCT taken at the same visit, were used in the analysis. Participants in the following 3 groups were analyzed: normal (N), perimetric glaucoma (PG), and pre-perimetric glaucoma (PPG). The eligibility criteria for the three groups analyzed are briefly described below, but were also described in our previous publication[16]. Further

description of the AIG Study protocol can be found in the AIGS Manual of Procedures (http://www.aigstudy.net/index.php?id=12, access March 18, 2009).

The N group participants had intraocular pressure (IOP) of less than 21 mm Hg for both eyes, a normal Humphrey SITA 24-2 standard visual field (VF) [mean deviation (MD) and pattern standard deviation (PSD) within 95% limits of the normal reference and a glaucoma hemifield test (GHT) within 97% limits], a central corneal thickness ≥ 500 μm, a normal-appearing optic nerve head, a normal nerve fiber layer, an open anterior chamber angle by gonioscopy, and no history of chronic ocular or systemic corticosteroid use.

The PG group participants had at least one eye that fulfilled the following criteria: glaucomatous (abnormal) VF loss [PSD ($P < 0.05$) or GHT ($P < 1\%$) outside normal limits in a consistent pattern on both qualifying VF's] and optic nerve head (ONH) changes such as diffuse or localized rim thinning, disc (splinter) hemorrhage, vertical cup/disc ratio greater than the fellow eye by > 0.2, or notch in the rim detected on baseline dilated fundus examination and confirmed by masked reading of stereo disc photographs.

The PPG group participants had same criteria for ONH change as defined for the PG group, but did not have the VF loss criteria need to meet eligibility for the PG group.

Exclusion criteria for all groups in the AIGS are: best-corrected visual acuity worse than 20/40; age < 40 or > 79 years; spherical equivalent refractive error > +3.00D or < −7.00 D; diabetic retinopathy or other diseases that could cause visual field loss or optic disc abnormalities; or previous intraocular surgery other than an uncomplicated cataract extraction with posterior chamber intraocular lens implantation.

The research was conducted in accordance with the Declaration of Helsinki. Informed consent was obtained from all participants after the goals of the study and consequences of participation had been discussed. The institutional review board of each institution involved in the study approved the research protocol.

Fourier-Domain Optical Coherence Tomography

Study participants were scanned using the RTVue FD-OCT system (Optovue, Inc. Fremont, CA), which acquires 26,000 axial scans (a-scans) per second and has a 5-μm depth resolution (full-width half-maximum) in tissue. With the FD-OCT, we devised three-dimensional scans of the macular region called the GCC scan that samples the macula with 14,928 a-scans over a 7 mm square area in 0.6 seconds (Fig. 2). We chose to limit the scan time to 0.6 second to reduce the problems of eye movement and corneal drying associated with long scan time. The scan pattern consists of 1 horizontal line and 15 vertical lines with 0.5 mm intervals. The center of the GCC scan is shifted 0.75 mm temporally to improve sampling of the temporal periphery.

Image Acquisition

All participants were scanned three times with the GCC scan (formerly called MM7 scan on software versions 3.0 and earlier). RTVue software versions 1.0 to V3.0 were used for acquisition. The photographers rejected scans with motion artifacts (discontinuous jump). The photographers did not look for signal strength or segmentation error because the processing software was not available at the time the study started. The OCT images were exported using the XML export function of RTVue version 3.0 software. The exported image set included 16 B-scans (cross-sectional images), each with 640×933 (depth×width) pixels and 3×7.5 micron pixel size. The entire set contains 9,553,920 pixels.

Participants were also scanned with the Stratus TD-OCT system (Carl Zeiss Meditec, Dublin, CA), which acquires 400 A-scans per second and has a 10-μm resolution. Stratus OCT imaging

was performed by the same photographer at the same visit using the fast retinal nerve fiber layer (RNFL) scan and the fast macular thickness map (FMTM) scan. The RNFL scan consists of three 3.4-mm circles around the optic disc. The FMTM scan contains six 6-mm radial scans. Both patterns contain 768 a-scans completed in 2 seconds. Two sets of both scans were taken in each eye. According to the AIGS protocol, photographer rejected scans with motion artifact, segmentation error (>15% consecutive or >20% cumulative number of A-scans with wrong boundary by visual inspection) or signal strength (SS) below 5 during the imaging session and took more scans to satisfy the criteria. For the purpose of this article, images with SS < 6 were further excluded. Using the standard Stratus 4.0 software, the overall averages of circumpapillary NFL thickness and macular retinal (MR) thicknesses were calculated.

Glaucoma severity was staged by MD and PSD according to the Glaucoma Staging System 2 (GSS2).[28]

Image Processing

We developed automated software to map GCC. First, the 15 vertical OCT cross-section images (Fig. 3A, available at http://aaojournal.org) were aligned in the z-dimension (depth axis) to the horizontal image by cross correlation to build a registered three-dimensional (3D) image set. To suppress background and speckle noises, each image was smoothed with a median filter.

To improve the speed and robustness of boundary detection, a progressive refinement procedure was applied. The procedure starts with boundary detection on a low-resolution (highly low-pass filtered) 3D data set and then progressively refines the boundary on progressively higher resolution (less filtered) data. A 2D version of this procedure was described in our previous work[16] and extended to 3D in the current algorithm.

The boundary detection algorithm starts with the photoreceptor pigment epithelium complex (PPC) band, which includes the bright bands of the photoreceptor inner segment-outer segment (IS/OS) junction and the retinal pigment epithelium. The PPC was detected as the second (counting from the inner side) maximum intensity peak in a low-resolution image (Fig. 3B, available at http://aaojournal.org). The IS/OS junction was then detected as the first maximum intensity peak within the PPC in the original resolution. Small portions of the PPC had low signal due to shadowing from overlying blood vessels; these shadowed a-scans were replaced by adjacent a-scans to avoid interruption of boundary detection. The images were aligned at the IS/OS junction to facilitate lateral smoothing. The gradient image was then obtained by applied gradient operator to smoothed intensity image in depth direction.

The inner limiting membrane (ILM) was identified as the first positive gradient peak of each A-scan. Neighbor constraint and a knowledge model were used to distinguish the ILM peak from spurious noise or detached vitreous face. The outer plexiform layer (OPL) were detected as the first intensity peak above (inner to) the IS/OS. Then the outer boundary of the inner plexiform layer (IPL) was identified as the negative gradient peak above the outer plexiform layer (OPL) peak (Fig. 3C, available at http://aaojournal.org). The accuracy of the segmentation was visually confirmed by author OT on every B-scan. If the segmentation of ILM, OPL, or IS/OS boundary was off by more than 5 pixels in more than 1/6 of any B-scan, the GCC scan was excluded. Based on the experience from visual inspection, we decided to reject images with signal strength index (SSI) below 38 because segmentation errors were too common below the SSI threshold.

The GCC thickness was measured from the ILM to the outer IPL boundary. Retinal thickness was measured from the ILM to the IS/OS junction. The GCC (Fig. 3D, available at http://aaojournal.org) and MR maps were computed by interpolation of the thickness profiles

from the 15 vertical B-scans in the 3D dataset. The interpolated map contain 933×933 points, which was interpolated from 933 A-scans × 15 B-scans (each B-scan contained 933 A-scans). The interpolation used cubic spline interpolation function in MATLAB. Finally, the position of the foveal depression was identified on the MR map and used to recenter the vertical position of the maps. The fovea center was identified as the location of minimal retinal thickness on the low-pass filtered map within 0.5 mm of fixation. The maps were cropped to remove peripheral areas where segmentation was less reliable. The remaining areas are those within a 7 mm diameter circle and within 3 mm from the central horizontal line. For the GCC map (Fig. 3E, available at http://aaojournal.org), the area within 0.75 mm of the foveal center (1.5 mm diameter circle) was also excluded because the GCC is too thin to be reliably measured in that region. The GCC maps of all eyes in the N group were averaged, point by point, to obtain the normal reference GCC map (Fig. 3F, available at http://aaojournal.org). The reference map is important for the calculation of GCC loss maps and pattern-based diagnostic parameters. The reference GCC map had a root-mean-square (RMS) standard deviation (SD) of 10 μm and standard error (SE) of 0.9 μm.

Derivation of Diagnostic Parameters

We computed several glaucoma diagnostic parameters based on the GCC map (Fig. 4A). The simplest was the overall average thickness (GCC-AVG). The difference between superior and inferior hemispheric averages (GCC-SID) was also computed.

To extract even more diagnostic information from the GCC map, we developed methods of analyzing the pattern of GCC loss. To do this, we computed maps of GCC loss: the fractional deviation (FD) map and the pattern deviation (PD) map. The FD map (Fig. 4B) is the GCC map minus the normal reference map divided by the normal reference map. The pattern map is the GCC thickness map normalized (divided) by its own overall average. The pattern deviation (PD) map (Fig. 4C) is the pattern map under consideration minus the normal reference pattern. The FD map shows the percentage of GCC loss. The PD map shows how the GCC pattern differs from normal.

Three pattern-based diagnostic parameters were then computed from the two derivative maps. The focal loss volume (FLV) is the sum FD in the region where there is significant focal loss. Significant focal loss is defined as PD more than 1.65 standard deviations (SD) below the normal average (below the fifth percentile of normal distribution). Global loss volume (GLV) is the sum of FD in areas where FD is negative. Pattern coefficient of variation (PCV) is the root mean square of the PD map.

The image processing and diagnostic parameter calculations were programmed in MATLAB 7.0 (The MathWorks, Natick, MA, U.S.A.).

Statistical Analyses

Both eyes of each participant were analyzed. The study sample was viewed as a clustered sample. The inter-eye correlation was accounted for in statistical tests by the use of a generalized estimating equation (GEE)[29] approach, linear mixed model[30], or formulas derived for clustered samples.[31–33]

To compare the means, a generalized linear model[34] with a GEE approach was used to evaluate the mean difference between groups. The p-values for mean comparisons were based on a Wald test.[35] The model allows for non-Gaussian distributions in addition to Gaussian distributions for fitting the dependent variables. The normality of distribution was verified by inspection of histogram and a Kolmogorov-Smirnov test. We noticed that some participants had one eye in PPG and the other eye in PG groups. To avoid the off calculation in model parameter estimation,

we compared PPG versus N, PG versus N respectively. The tests were performed in a one-tailed manner since we hypothesize that the means in the diseased groups are lower than in the normal group.

Intraclass correlation(ICC),[36] pooled SD,[37] and coefficient of variation (CV) were used to evaluate the reproducibility of diagnostic parameters. These indices were computed from linear mixed models in which the variance components for subject and eye variation were included to account for intra-subject correlation. . To compare pooled SD or CV between diagnostic parameters, we generated the pooled SD or CV for each eye and used GEE paired t-tests for comparisons.

Area under the receiver operating characteristic (AROC) curve was used to compare diagnostic power. To account for inter-eye correlation, the AROC was computed based on the formula of Obuchowski,[33] which extended the nonparametric method of Delong et al.[38] as applied to clustered data. The same method has been used in previous studies in ophthalmology[16, 39] to handle inter-eye correlation.

To adjust for age imbalance between the N, PG, and PPG groups, a logistic regression model with age and diagnostic parameter in covariates was used to generate the AROC. This method of compensating for age imbalance has been used in a previous ophthalmology study.[40] A GEE approach was added to the logistic regression model to account for the inter-eye correlation in the study sample.

For sensitivity and specificity, we computed thresholds for 5th and 1st percentiles. For a Gaussian distributed parameter, the percentiles can be formulated as $\text{mean}_N + Z_\alpha \text{SD}_N$, where mean_N and SD_N are the mean and standard deviation of the normal group, $Z_\alpha = -1.65$ for the fifth percentile cutoff, and $Z_\alpha = -2.33$ for the first percentile cutoff. The parametric distribution of a non-Gaussian parameter was estimated based on 10,000 replicates, in which one eye was randomly selected from each participant. The SD_N and the standard error of sensitivity and specificity were computed based on the formulas for clustered data[31, 32], this method has been used in previous studies in ophthalmology[16, 39].

The AROC calculations were written in MATLAB 7.0 software and the other statistical calculations were performed with the SAS 9.1 software. The critical alpha level of statistical significance was set at 0.05.

Results

A total of 183 participants (328 eyes) with available RTVue GCC and Stratus scans were identified from the AIG central database. A total of 849 GCC scans were screened, 48 were excluded for low signal and 41 were excluded due to segmentation error. The average SSI of the accepted GCC scans was 39.8. A total of 622 Stratus scans were screened, 12 scans were excluded due to low signal strength. The average SS of the accepted Stratus scans was 8.3. Stratus scans that had segmentation error were rejected and retaken by the photographer so a failure rate was not available. Finally, 18 eyes were excluded due to lack of valid FD-OCT or TD-OCT data. The remaining 310 eligible eyes from 178 participants were analyzed. The demographic and clinical information for each group were summarized in Table 1. Pre-perimetric glaucoma and PG participants were both significantly older than N participants by approximately 7 years. The potential overestimation of AROC due to the age imbalance was removed using a logistic regression model as stated in the methods section. There were more Caucasians in the N group compared to PG group. However, there was no significant difference between the racial groups in terms of the means of diagnostic parameters in the N group. The PG group had significantly thinner central corneal thickness than the N group and the PPG group had significantly higher IOP than the N group. Both PG and PPG groups had significantly

worse VF parameters than the N group. All participants had open angles by gonioscopy except one participant with narrow angles in the PPG group.

According GSS2 system, the 109 PG eyes were classified into stage 0 (18 eyes), borderline (14 eyes), stage 1 (20 eyes), stage 2 (17 eyes), stage 3 (20 eyes), stage 4 (16 eyes) and stage 5 (4 eyes). Forty one eyes had localized defects, 24 eyes have mixed defects and 12 eyes have generalized defects. Seventy nine eyes (70.5%) had MD ≥−6.0 dB, 25 eyes (22.3%) had MD between −6.01 to −12.0 dB, and 8 eyes (7.1%) MD < −12dB.

Table 2 summarized the distribution statistics of each diagnostic parameter by group. All parameters were significantly worse in the PPG and PG groups compared to the N group ($P < 0.001$). Because SID, PCV, FLV and GLV had non-normal distributions (Gamma distributions), these parameters were compared using the Wald test as described in the methods section.

Repeatability was assessed by three measures: ICC, pooled SD, and CV of repeated measures (Table 3, available at http://aaojournal.org) during the same session. The repeatability in the PPG and PG groups is important because it provides an indication of how well a parameter can track progression through stages of the disease. Because glaucoma primarily affects the GCC (inner 3 retinal layers), it should affect GCC thickness and MR thickness in parallel fashion, matching μm by μm. Thus their relative precision in tracking glaucoma can be gauged by the pooled SD. The pooled SDs of FD-OCT GCC were significantly smaller than TD-OCT MR in the N ($p = .005$) and PG ($p = 0.02$) groups. The pooled SDs of FD-OCT MR were also significantly smaller than TD-OCT MR in the N ($p = 0.002$) and PG ($p = 0.048$) groups. In PPG group, the p-values were close to statistical significance (0.08 for GCC and 0.07 for MR). We cannot assume that glaucoma would affect GCC and NFL the same μm by μm, but their loss might be roughly proportional. Therefore CV could provide an approximate comparison between the repeatability of GCC and NFL. The CV's of FD-OCT GCC were significantly smaller than TD-OCT NFL in the N ($p = 0.0002$) and PG ($p < 0.001$) groups but not in the PPG group ($p=0.11$). To compare the repeatability of all FD-OCT parameters, it is best to use ICC, because the pattern parameters (FLV, GLV, PCV, SID) have mean values close to zero (therefore CV's are not meaningful) and have different units (therefore SD's are not comparable). The FD-OCT GCC-AVG, GCC-GLV, and MR-AVG all have the highest ICC values of 0.99 in the PG and PPG groups and therefore may be the best parameters to watch for the tracking of glaucoma progression.

The AROC (Table 4) provided a summary measure of the accuracy of diagnosing glaucoma against the normal reference group. The MR average measured by FD-OCT and TD-OCT had equivalent AROC values. By isolating the inner retina, GCC-AVG significantly improved the diagnosis of PG (AROC = 0.90) compared to MR ($p = 0.021$). The pattern parameter GCC-GLV ($p = 0.01$) performed even better in diagnosing PG than GCC. The macular parameters GCC-AVG, GCC-FLV, GCC-GLV had statistically equal ($p > 0.1$) diagnostic power compared to NFL-AVG. For the diagnosis of PPG (versus N), we found no significant difference between GCC parameters and MR. Diagnostic accuracy is also shown in the form of diagnostic sensitivities at 1^{st} and 5^{th} percentile cutoff thresholds (Table 5).

The odds ratio (95% confidence interval) of having glaucoma for every 10 μm loss of tissue was 7.45 (4.14, 13.40) for GCC-AVG, 5.06 (2.58, 9.92) for NFL and 2.69 (1.96, 3.67) and 2.53 (1.84, 3.47) for FD-OCT and TD-OCT MR, respectively. We note that for each 10-μm of tissue loss, GCC predicts a significantly larger (3-fold) increase in the odds ratio than the loss of MR.

We chose a PG case with a very asymmetric VF to show how the locations of VF and disc rim defects correlated with GCC loss (Fig. 4). The predominantly inferior GCC loss correlated with the inferior disc rim loss and superior VF defect.

The pattern of GCC loss averaged over the PG group (Fig. 5) showed sparing of the maculopapillar bundle, which was tilted in accordance with the fact that the fovea is below the level of the disc. The severest fractional loss occurred at the superior and inferior edges of the map, corresponding to the locations of the superior and inferior arcuate NFL bundles.

We chose a PPG case (Fig. 6, available at http://aaojournal.org) where the average GCC was within normal and the pattern parameters were abnormal, to investigate how such a situation could arise. In this case, the GCC loss was localized primarily to an area above the fovea, and the abnormality was easily picked up by the pattern-based parameters. But the GCC was actually thicker than average in the maculopapillar area, which contributed toward an average GCC thickness that was still within the normal range. The focal loss of GCC in the superior macula was as much as 30%, corresponding to a mild thinning of the superotemporal disc rim, while the VF was essentially normal.

To investigate whether GCC can help detect glaucomatous abnormalities not picked up by NFL, we constructed Venn diagrams of GCC and NFL abnormalities in both the PG and PPG groups (Fig. 7). We combined the 3 best GCC parameters – GCC abnormality was defined as GCC-AVG, FLV or GLV below fifth percentile of the normal reference. Abnormal NFL was defined by NFL-AVG below fifth percentile. GCC detected additional 9% of PG cases and 11% of PPG cases that were not detected by NFL.

Discussion

Although glaucoma is clinically defined as optic disc cupping with corresponding visual field defects, the underlying disease process in glaucoma is the loss of RGC.[1–3] Approximately one-third of the RGC population resides within the posterior pole. In the macula, the RGC layer is more than one cell layer thick with an RGC body diameter 10 to 20 times larger compared to their axons. In addition, the central retina has less variability in cell density compared with peripheral retina.[41] Thus detecting RGC loss in the macula may allow earlier detection of glaucoma in some cases.

Ishikawa et al.[15] developed a software algorithm to perform automatic retinal layer segmentation in the macula for the commercially available Stratus TD-OCT and reported that macular inner retinal layer thickness measurements could indeed be used to discriminate normal from glaucomatous eyes. They found that the outer retinal layers were not affected in glaucoma. However, one of the limitations of the study was variable scan quality. Over one-third of their scans on glaucomatous eyes had to be excluded from segmentation analysis due to poor quality scans related to speckle noise and uneven tissue reflectivity. The authors suggested that higher resolution and improved signal quality (higher signal-to-noise ratio), as provided by FD-OCT, may be needed for better quality image acquisition to allow accurate retinal layer segmentation.

Leung et al[42] used the Stratus TD-OCT to evaluate macular NFL thinning in glaucoma using the 3.4-mm diameter circular scan pattern (Fast RNFL scan). They reported a reduction in macular NFL thickness in glaucomatous eyes compared with normal eyes. However, they found that measurement of macular NFL thickness offered no advantage over measurement of total macular thickness for glaucoma detection. In their study, circumpapillary NFL thickness outperformed macular NFL and total macular thickness in the ability to detect glaucoma and correlate with visual function.

Greenfield et al[43] reported that OCT-derived macular thickness was well correlated with changes in visual function and RNFL structure in moderately advanced glaucoma. They reported a strong correlation between mean macular thickness and visual field mean deviation (R^2=0.47, p<0.001), and suggested that reduced macular thickness could be a surrogate for loss of RGCs in glaucoma.

Our study confirmed that MR thickness by either FD-OCT or Stratus TD-OCT was a less accurate parameter for glaucoma detection than Stratus NFL thickness. Other investigators, including Wollestein et al[13], Guedes et al,[44] and Medeiros et al[45] have also reported higher AROC values for Stratus NFL compared with Stratus MR for glaucoma detection. Our AROC values for MR by TD-OCT (AROC 0.85) and FD-OCT (AROC 0.85) were slightly higher than values previously reported by Medeiros et al (AROC 0.75 – 0.81)[45].

In the current study, we report on the development of novel diagnostic parameters using FD-OCT to look for glaucoma in the macula. The faster speed of FD-OCT (65× Stratus TD-OCT) allows high density scanning over a large region of the macula with less motion artifact. The resolution of the RTVue FD-OCT device is also two times better than Stratus TD-OCT. The combination of higher definition (denser sampling) and higher resolution significantly improved the precision (repeatability) of both MR and GCC measurement, which could improve the ability to track glaucomatous thinning over time.

Our study also showed that the GCC average measured by the RTVue FD-OCT were significantly better at diagnosing glaucoma in the PG group, compared to the MR average measured by either FD-OCT or TD-OCT. Thus, isolating GCC from the outer retina improved the diagnostic power of the macular measurement. This could be explained by the fact that the outer retina, which is not much affected by glaucoma, takes up 65% to 70% of total retinal thickness and, therefore, could contribute variation in thickness that decreases discriminant power. The diagnostic power of GCC average was also higher than that of MR in the discrimination between PPG and N eyes, but the advantage was not statistically significant. This could be explained by the smaller PPG group size. Also, the PPG group is primarily defined by detection of rim notching on disc photographs, which may bias the diagnosis toward those with rim loss primarily in the superior and inferior poles of the optic nerve head, while missing those with rim thinning more temporally. So the PPG group may have a lower percentage of cases with significant macular ganglion cell loss. Macular GCC measurement by OCT may detect pre-perimetric glaucoma earlier in those cases where the ganglion cell loss is more predominantly macular rather than peripheral. We will study this possibility in a group of ocular hypertensives and other glaucoma suspects enrolled in the AIGS.

Our study showed that FD-OCT macula GCC parameters did not have higher AROC than TD-OCT circumpapillary NFL – they were statistically equal. This is understandable as the circumpapillary NFL samples nearly all axons arising from ganglion cells, while the GCC scan only covers the macular area. On the other hand, the GCC scan samples the macula better and may be able to better detect glaucoma cases where macular loss occur early. Thus GCC and NFL parameters may be complementary. In our preliminary investigation with the Venn diagram (Figure 7), the addition of GCC data to NFL increased detection rate from 78% to 87% in the PG group and from 45% to 56% in the PPG group. We will further study if a composite parameter incorporating both FD-OCT NFL and GCC parameters could significantly increase diagnostic accuracy. The combination of diagnostic parameters from different anatomic areas have been found to boost diagnostic accuracy in previous studies[39, 46]

Wider and finer sampling of the macular regions in less than 1 second was made possible by the higher speed of FD-OCT. This facilitated the analysis of patterns of GCC loss. We designed

several pattern-based parameters that looked at different aspects of the GCC loss pattern and have the potential to be utilized in a complementary fashion. The SID parameter was designed to detect cases where GCC loss is asymmetric between superior and inferior macular regions. The GLV and FLV parameters sum up the volume of GCC loss in the macula with differing levels of focality. The FLV parameter is more focal because it only sums loss in regions where the GCC is thin in both absolute (GCC < normal) and relative (PD < 5^{th} percentile) terms. The PCV parameter is purely based on the PD map and detects any change in the GCC pattern. We found that FLV and GLV had higher diagnostic accuracy than the simple average for the diagnosis of PG. This must mean that in some cases pattern parameters are more sensitive or more specific. For example, pattern parameters could be more sensitive in eyes that have started with an above average GCC thickness and where GCC loss is focal rather than diffuse (example shown in Fig. 6). Pattern parameters could be more specific in a normal eye that had baseline thinner GCC with normal distribution pattern.

An advantage of the GCC map is that it could be correlated with VF defects point-by-point. When they correspond, one may be more confident that the defects are real rather than artifacts. An example of this correspondence was shown in Fig. 4. It is important to note that each millimeter on the retina corresponds to about 3.5° on the VF. Therefore the GCC map (7 mm × 6 mm) subtends about 11° superiorly and inferiorly, 10° nasally, and 15° temporally. It covers about half of the area of the standard Humphrey 24-2 VF (Figs. 4E), and, of course, is up/down reversed relative to the VF due to optical projection in the eye. The example in Fig. 4 showed that in the case of end-stage VF defect (−35 dB), the fractional GCC loss was approximately 50%. Possibly residual glial tissue maintains 50% thickness even when nearly all ganglions cells were lost.

One of the limitations of the study is that the normal group was used to both define the normal reference GCC pattern and assess diagnostic specificity. This could theoretically cause a false inflation of the specificity and AROC values of the GCC pattern parameters. However, we believe this effect was probably very small because there is no reason why the GCC distribution pattern would vary between normal populations, and we had a sufficient number of normal participants to obtain a smooth normal reference GCC map (Fig. 3F) with a tight SE of 0.9 μm. Nevertheless, a separate study with an independent population is needed to confirm our conclusions. The GCC segmentation and the pattern parameters described here have been licensed to Optovue, Inc. The GCC map and average was released in RTVue software version 3.0 and the pattern parameters were released in version 4.0. We invite other investigators to use the commercially released software to validate our findings.

In summary, we found that GCC measurements with FD-OCT have better diagnostic accuracy and repeatability compared with MR measurements by either TD-OCT or FD-OCT. Analysis of GCC loss pattern further boosted diagnostic accuracy. Independent investigations are needed to validate the findings of this pilot study.

Acknowledgments

Supported by NIH grants R01 EY013516 and P30 EY03040, a grant from Research to Prevent Blindness, and a grant from Optovue, Inc.

References

1. Quigley HA, Dunkelberger GR, Green WR. Retinal ganglion cell atrophy correlated with automated perimetry in human eyes with glaucoma. Am J Ophthalmol 1989;107:453–464. [PubMed: 2712129]
2. Quigley HA, Miller NR, George T. Clinical evaluation of nerve fiber layer atrophy as an indicator of glaucomatous optic nerve damage. Arch Ophthalmol 1980;98:1564–1571. [PubMed: 7425916]

3. Sommer A, Miller NR, Pollack I, et al. The nerve fiber layer in the diagnosis of glaucoma. Arch Ophthalmol 1977;95:2149–2156. [PubMed: 588106]
4. Sommer A, Quigley HA, Robin AL, et al. Evaluation of nerve fiber layer assessment. Arch Ophthalmol 1984;102:1766–1771. [PubMed: 6508617]
5. Pederson JE, Anderson DR. The mode of progressive disc cupping in ocular hypertension and glaucoma. Arch Ophthalmol 1980;98:490–495. [PubMed: 7362506]
6. Sommer A, Katz J, Quigley HA, et al. Clinically detectable nerve fiber atrophy precedes the onset of glaucomatous field loss. Arch Ophthalmol 1991;109:77–83. [PubMed: 1987954]
7. Quigley HA, Katz J, Derick RJ, et al. An evaluation of optic disc and nerve fiber layer examinations in monitoring progression of early glaucoma damage. Ophthalmology 1992;99:19–28. [PubMed: 1741133]
8. Airaksinen PJ, Drance SM, Douglas GR, et al. Diffuse and localized nerve fiber loss in glaucoma. Am J Ophthalmol 1984;98:566–571. [PubMed: 6496612]
9. Harwerth RS, Carter-Dawson L, Shen F, et al. Ganglion cell losses underlying visual field defects from experimental glaucoma. Invest Ophthalmol Vis Sci 1999;40:2242–2250. [PubMed: 10476789]
10. Zeimer R, Asrani S, Zou S, et al. Quantitative detection of glaucomatous damage at the posterior pole by retinal thickness mapping: a pilot study. Ophthalmology 1998;105:224–231. [PubMed: 9479279]
11. Huang D, Swanson EA, Lin CP, et al. Optical coherence tomography. Science 1991;254:1178–1181. [PubMed: 1957169]
12. Bagga H, Greenfield DS, Knighton RW. Macular symmetry testing for glaucoma detection. J Glaucoma 2005;14:358–363. [PubMed: 16148583]
13. Wollstein G, Schuman JS, Price LL, et al. Optical coherence tomography (OCT) macular and peripapillary retinal nerve fiber layer measurements and automated visual fields. Am J Ophthalmol 2004;138:218–225. [PubMed: 15289130]
14. Lederer DE, Schuman JS, Hertzmark E, et al. Analysis of macular volume in normal and glaucomatous eyes using optical coherence tomography. Am J Ophthalmol 2003;135:838–843. [PubMed: 12788124]
15. Ishikawa H, Stein DM, Wollstein G, et al. Macular segmentation with optical coherence tomography. Invest Ophthalmol Vis Sci 2005;46:2012–2017. [PubMed: 15914617]
16. Tan O, Li G, Lu AT, et al. Mapping of macular substructures with optical coherence tomography for glaucoma diagnosis. Ophthalmology 2008;115:949–956. [PubMed: 17981334]
17. Wojtkowski M, Srinivasan V, Fujimoto JG, et al. Three-dimensional retinal imaging with high-speed ultrahigh-resolution optical coherence tomography. Ophthalmology 2005;112:1734–1746. [PubMed: 16140383]
18. Leitgeb R, Hitzenberger CK, Fercher AF. Performance of Fourier domain vs. time domain optical coherence tomography. Opt Express [serial online]. 2003 11:889–894.Available at: http://www.opticsinfobase.org/oe/abstract.cfm?uri=oe-11-8-889
19. Choma MA, Sarunic MV, Yang C, Izatt JA. Sensitivity advantage of swept-source and Fourier domain optical coherence tomography. Opt Express [serial online]. 2003 11:2183–2189.Available at: http://www.opticsinfobase.org/oe/abstract.cfm?uri=oe-11-18-2183
20. Wojtkowski M, Leitgeb R, Kowalczyk A, et al. In vivo human retinal imaging by Fourier domain optical coherence tomography. J Biomed Opt 2002;7:457–463. [PubMed: 12175297]
21. Wojtkowski M, Kowalczyk A, Leitgeb R, Fercher AF. Full range complex spectral optical coherence tomography technique in eye imaging. Opt Lett 2002;27:1415–1417. [PubMed: 18026464]
22. de Boer JF, Cense B, Park BH, et al. Improved signal-to-noise ratio in spectral-domain compared with time-domain optical coherence tomography. Opt Lett 2003;28:2067–2069. [PubMed: 14587817]
23. Wojtkowski M, Bajraszewski T, Targowski P, Kowalczyk A. Real-time in vivo imaging by high-speed spectral optical coherence tomography. Opt Lett 2003;28:1745–1747. [PubMed: 14514087]
24. Yun SH, Tearney GJ, Bouma BE, et al. High-speed spectral-domain optical coherence tomography at 1.3 mum wavelength. Opt Express [serial online]. 2003 11:3598–3604.Available at: http://www.opticsinfobase.org/oe/abstract.cfm?uri=oe-11-26-3598

25. Nassif N, Cense B, Park BH, et al. In vivo human retinal imaging by ultrahigh-speed spectral domain optical coherence tomography. Opt Lett 2004;29:480–482. [PubMed: 15005199]
26. Nassif NA, Cense B, Park BH, et al. In vivo high-resolution video-rate spectral-domain optical coherence tomography of the human retina and optic nerve. Opt Express [serial online]. 2004 12:367–376.Available at: http://www.opticsinfobase.org/oe/abstract.cfm?uri=oe-12-3-367
27. Chen TC, Cense B, Pierce MC, et al. Spectral domain optical coherence tomography: ultra-high speed, ultra-high resolution ophthalmic imaging. Arch Ophthalmol 2005;123:1715–1720. [PubMed: 16344444]
28. Brusini P, Filacorda S. Enhanced Glaucoma Staging System (GSS 2) for classifying functional damage in glaucoma. J Glaucoma 2006;15:40–46. [PubMed: 16378017]
29. Liang KY, Zeger SL. Longitudinal data analysis using generalized linear models. Biometrika 1986;73:13–22.
30. Laird NM, Ware JH. Random-effects models for longitudinal data. Biometrics 1982;38:963–974. [PubMed: 7168798]
31. Williams RL. A note on robust variance estimation for cluster-correlated data. Biometrics 2000;56:645–646. [PubMed: 10877330]
32. Rao JN, Scott AJ. A simple method for the analysis of clustered binary data. Biometrics 1992;48:577–585. [PubMed: 1637980]
33. Obuchowski NA. Nonparametric analysis of clustered ROC curve data. Biometrics 1997;53:567–578. [PubMed: 9192452]
34. McCullagh, P.; Nelder, J. Monographs on Statistics and Applied Probability. Vol. 2nd ed.. Vol. vol. 37. London: Chapman and Hall; 1989. Generalized Linear Models; p. 21-44.
35. Snijders, T.; Bosker, R. Multilevel Analysis: An Introduction to Basic and Advanced Multilevel Modeling. London: Sage Publ.; 1999. p. 86
36. Cinelli RA, Tozzini V, Pellegrini V, et al. Coherent dynamics of photoexcited green fluorescent proteins. Phys Rev Lett 2001;86:3439–3442. [PubMed: 11327990]
37. Warmke J, Drysdale R, Ganetzky B. A distinct potassium channel polypeptide encoded by the *Drosophila eag* locus. Science 1991;252:1560–1562. [PubMed: 1840699]
38. DeLong ER, DeLong DM, Clarke-Pearson DL. Comparing the areas under two or more correlated receiver operating characteristic curves: a nonparametric approach. Biometrics 1988;44:837–845. [PubMed: 3203132]
39. Lu AT, Wang M, Varma R, et al. Advanced Imaging for Glaucoma Study Group. Combining nerve fiber layer parameters to optimize glaucoma diagnosis with optical coherence tomography. Ophthalmology 2008;115:1352–1357. [PubMed: 18514318]
40. Deleon-Ortega JE, Arthur SN, McGwin G Jr, et al. Discrimination between glaucomatous and nonglaucomatous eyes using quantitative imaging devices and subjective optic nerve head assessment. Invest Ophthalmol Vis Sci 2006;47:3374–3380. [PubMed: 16877405]
41. Glovinsky Y, Quigley H, Pease ME. Foveal ganglion cell loss is size dependent in experimental glaucoma. Invest Ophthalmol Vis Sci 1993;34:395–400. [PubMed: 8440594]
42. Leung CK, Chan WM, Yung WH, et al. Comparison of macular and peripapillary measurements for the detection of glaucoma: an optical coherence tomography study. Ophthalmology 2005;112:391–400. [PubMed: 15745764]
43. Greenfield DS, Bagga H, Knighton RW. Macular thickness changes in glaucomatous optic neuropathy detected using optical coherence tomography. Arch Ophthalmol 2003;121:41–46. [PubMed: 12523883]
44. Guedes V, Schuman JS, Hertzmark E, et al. Optical coherence tomography measurement of macular and nerve fiber layer thickness in normal and glaucomatous human eyes. Ophthalmology 2003;110:177–189. [PubMed: 12511364]
45. Medeiros FA, Zangwill LM, Bowd C, et al. Evaluation of retinal nerve fiber layer, optic nerve head, and macular thickness measurements for glaucoma detection using optical coherence tomography. Am J Ophthalmol 2005;139:44–55. [PubMed: 15652827]
46. Zangwill LM, Chan K, Bowd C, et al. Heidelberg retina tomography measurements of the optic disc and parapapillary retina for detecting glaucoma analyzed by machine learning classifiers. Invest Ophthalmol Vis Sci 2004;45:3144–3151. [PubMed: 15326133]

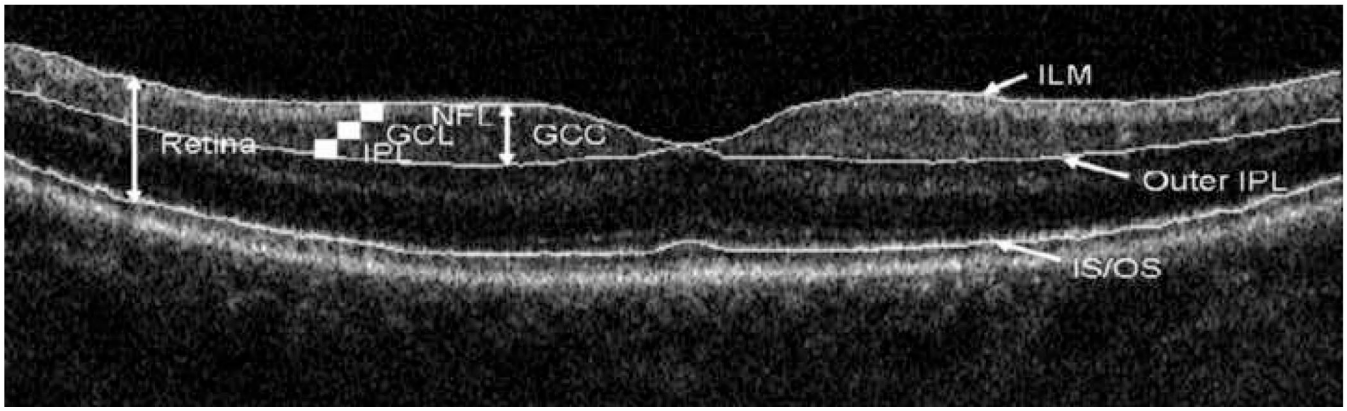

Figure 1.
Vertical optical coherence tomography (OCT) cross section of the macula. The image was acquired using the RTVue Fourier-domain (FD) OCT system. The ganglion cell complex (GCC) consists of 3 layers: nerve fiber layer (NFL), ganglion cell layer (GCL) and inner plexiform layer (IPL). The three boundaries on the image are inner limiting membrane (ILM), outer IPL boundary and inner segment/outer segment (IS/OS) junction. The GCC thickness is measured from the ILM to the outer IPL boundary. The retinal thickness is measured from the ILM to the IS/OS junction.

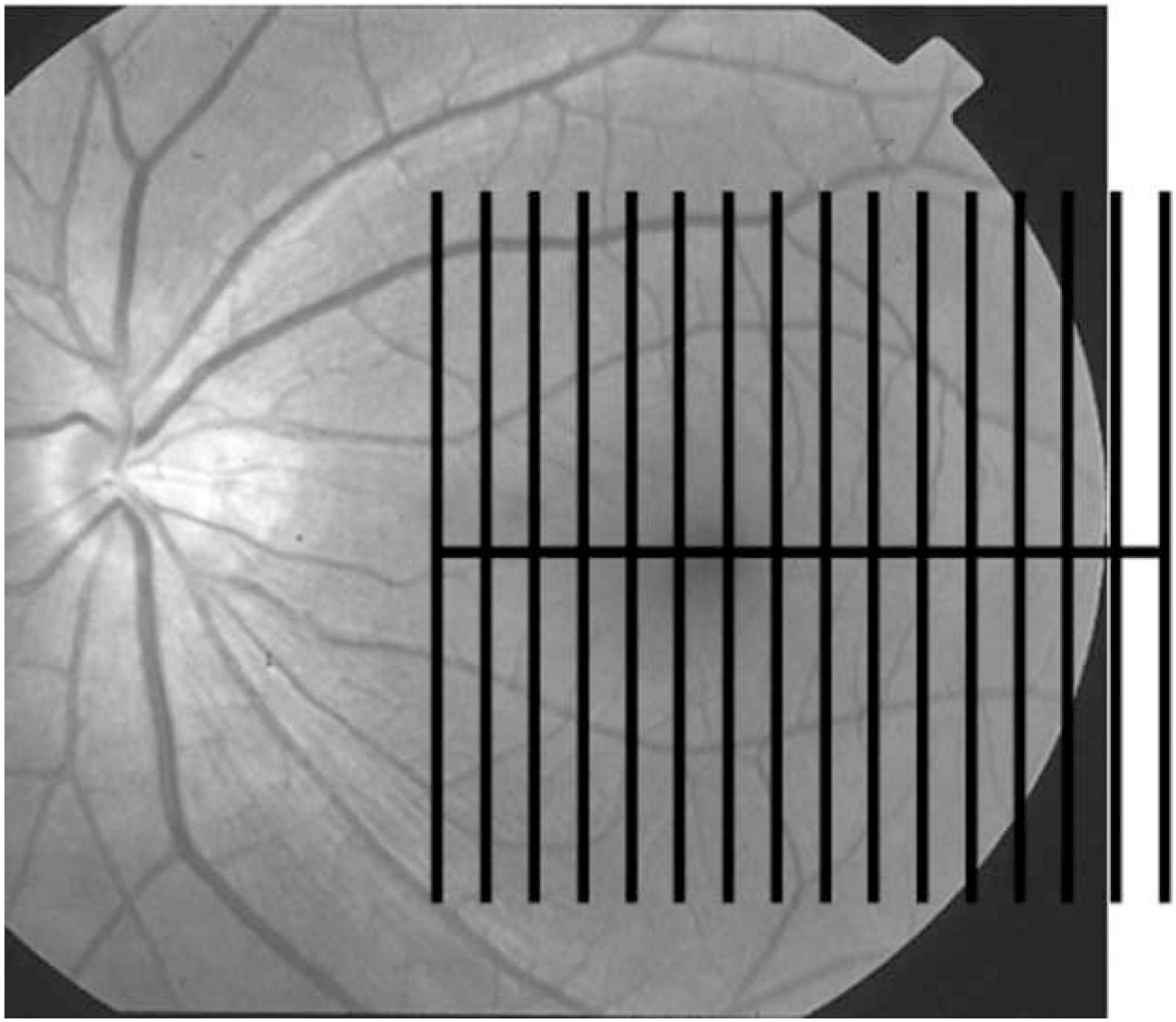

Figure 2.
The ganglion cell complex (GCC) scan pattern consists of 15 vertical and 1 horizontal scan lines shown overlaid on a red-free fundus photograph.

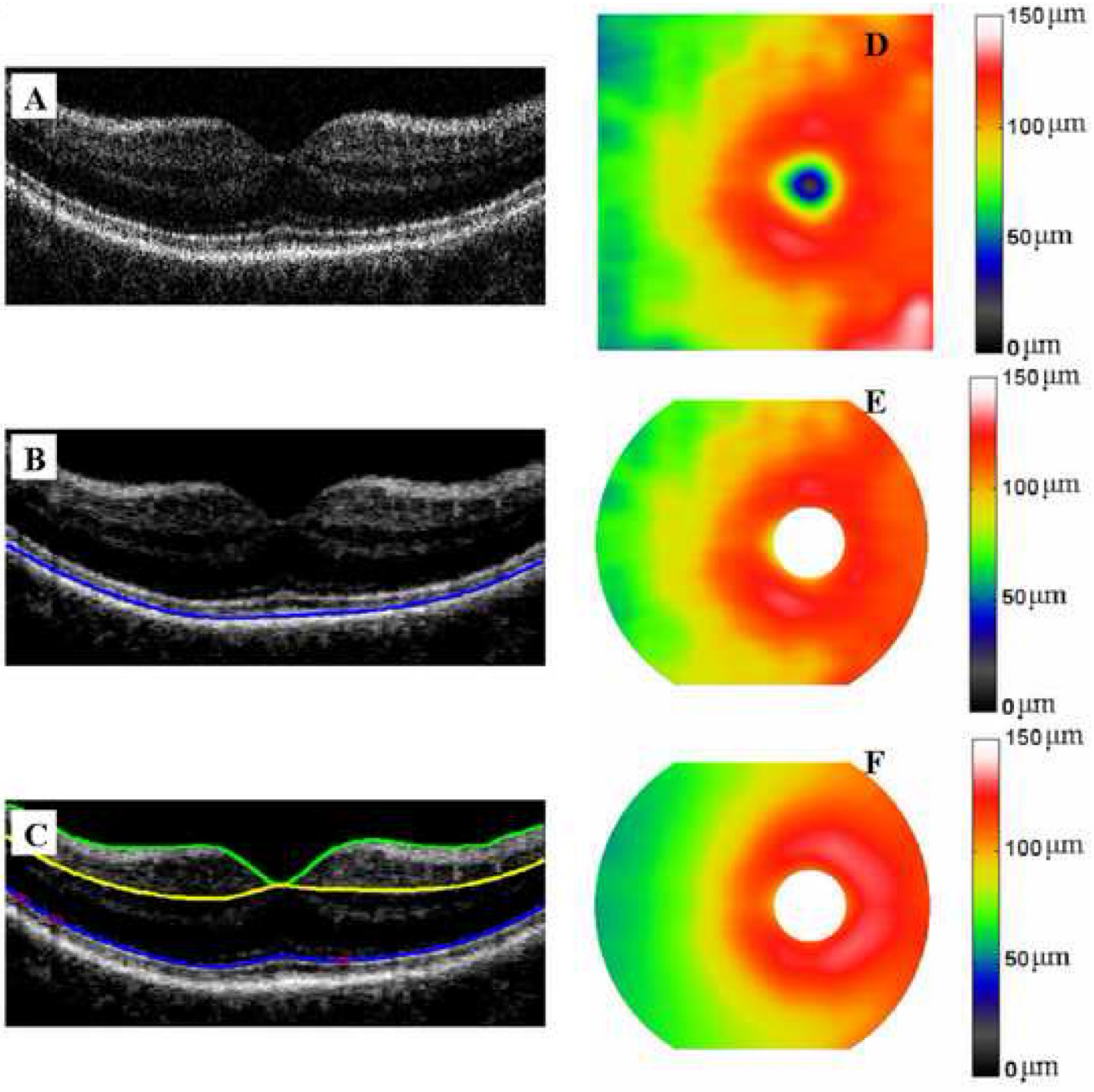

Figure 3.

Image processing steps in the automated measurement of ganglion cell complex (GCC) and retinal thickness. (A) A vertical optical coherence tomography (OCT) cross-section from the GCC scan is shown. (B) The OCT image was low-pass filtered and re-sampled at lower definition to suppress speckle and speed processing. The photoreceptor pigment-epithelium complex (PPC, blue line) was identified. (C) The inner segment/outer segment (IS/OS) junction (blue line) was detected from within the PPC. The inner limited membrane (ILM, green line) and outer boundary of the outer plexiform layer (OPL, yellow line) were also detected. Blood vessel shadowed axial-scans (A-scans, red circle) were replaced with adjacent A-scans to avoid interruption of boundary lines. (D) Macular GCC thickness map was obtained by interpolation

of the GCC profiles from the 16 OCT cross-sections in the GCC scan pattern. (E) The GCC map was re-centered on the foveal depression. Unreliable portions of the map were removed (cropped out on map shown). These include the foveal area (1.5 mm diameter); top and bottom 0.5mm; and the corner regions with distance from map center > 3.5mm. (F) The reference GCC map is averaged from all eyes in the normal (N) group.

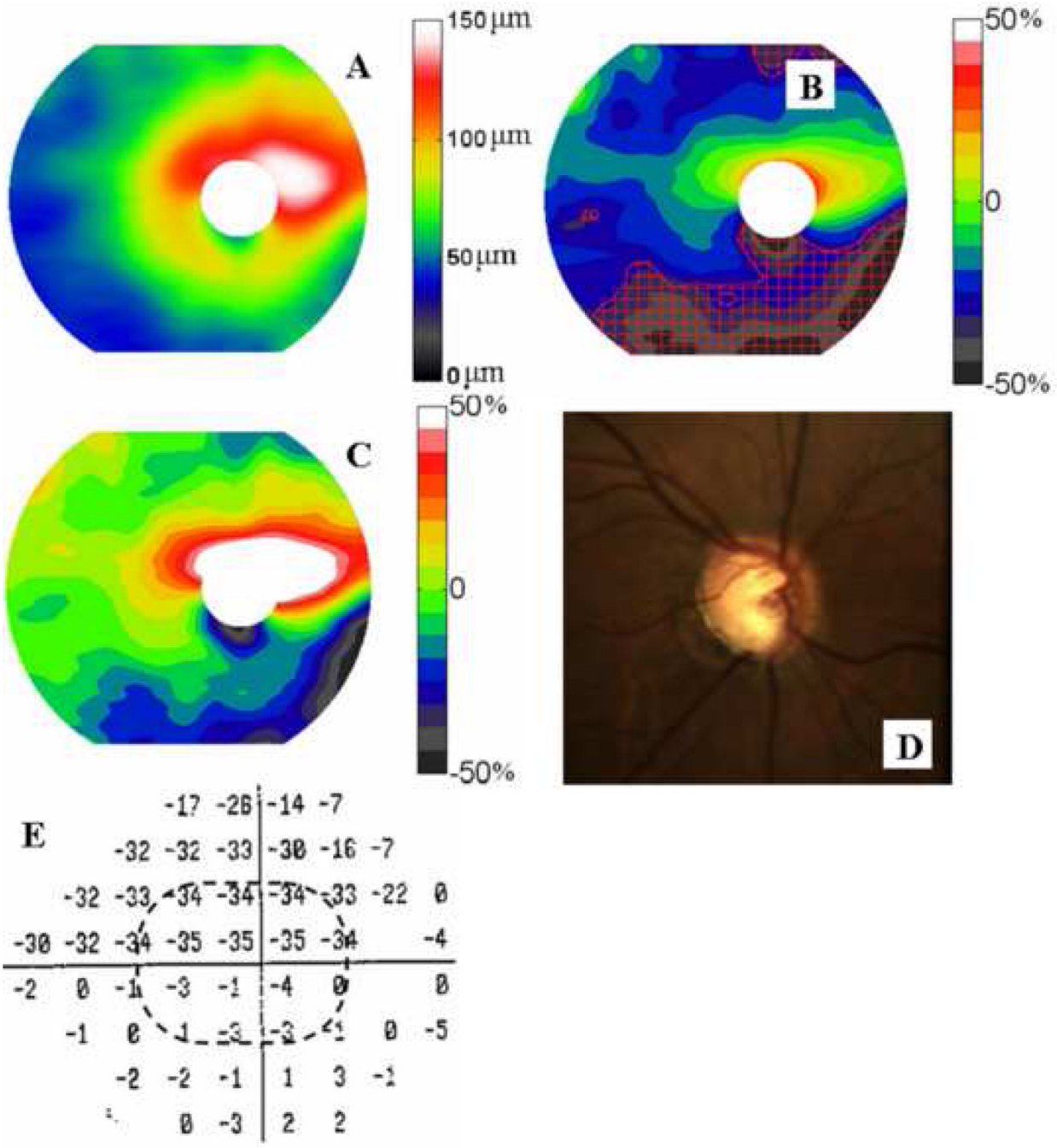

Figure 4.

A perimetric glaucoma (PG) case example. All of the ganglion cell complex (GCC) parameters were abnormal (average = 71 µm, $p < 0.5\%$; focal loss volume (FLV) =12.6%, $p < 0.5\%$, global loss volume (GLV) = 26.5%, $p < 0.5\%$; pattern coefficient of variation (PCV) = 21%, $p < 0.5\%$; superior-inferior difference (SID) = 17.0 µm, $p < 0.5\%$). (A) GCC map. (B) Fractional deviation map with areas of significant focal loss marked by red hatching. (C) GCC pattern deviation (PD) map. (D) Disc photo showing inferotemporal rim loss. (E) Visual field (VF) PD map. The VF was abnormal (pattern standard deviation = 16.5dB, $p < 0.5\%$; glaucoma hemifield test was outside normal limits. The elliptical dashed line shows the area

corresponding to the GCC maps. The superior VF defect corresponded to the inferior GCC loss and disc rim thinning.

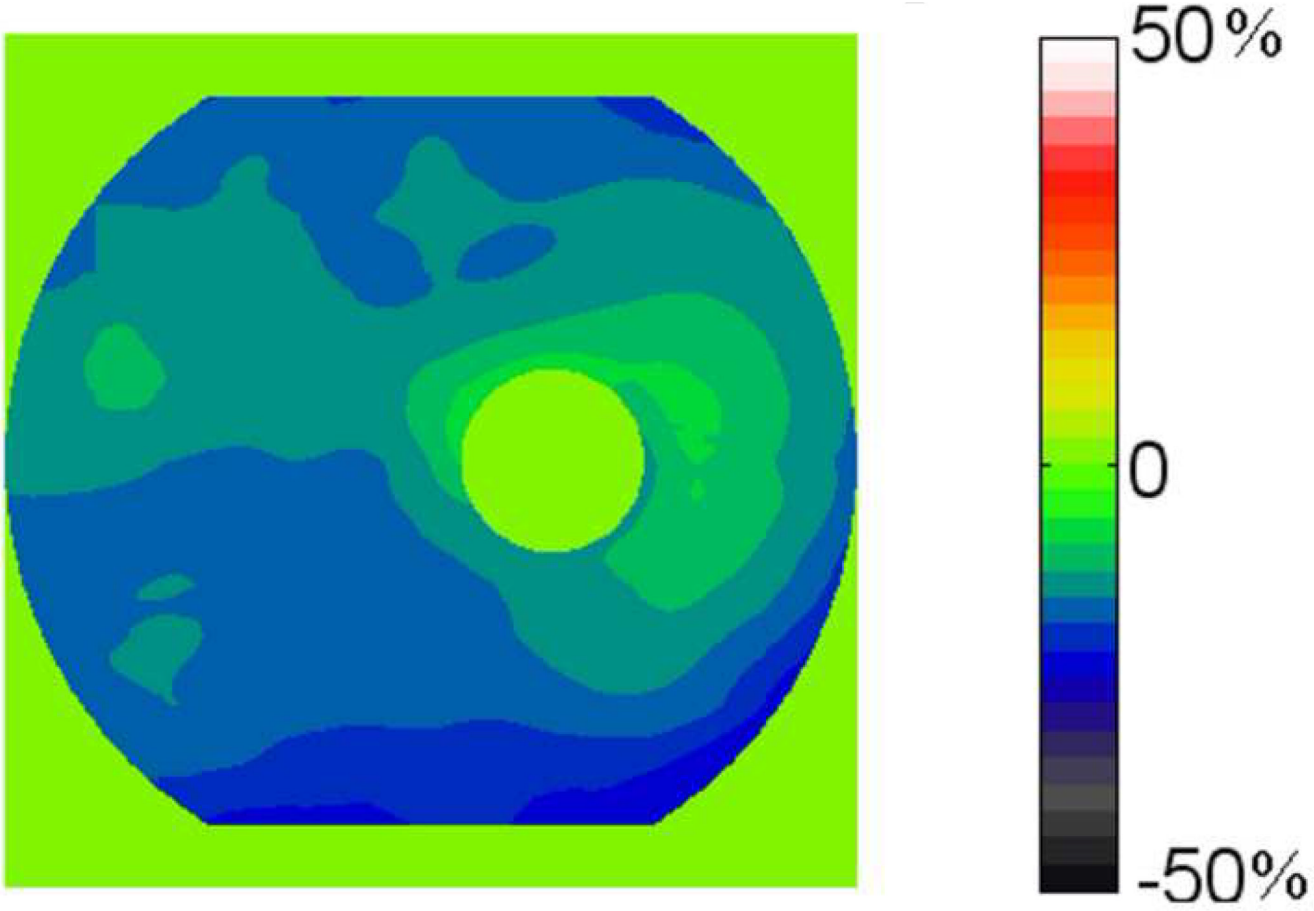

Figure 5.
The average ganglion cell complex (GCC) fractional deviation map of the perimetric glaucoma (PG) group.

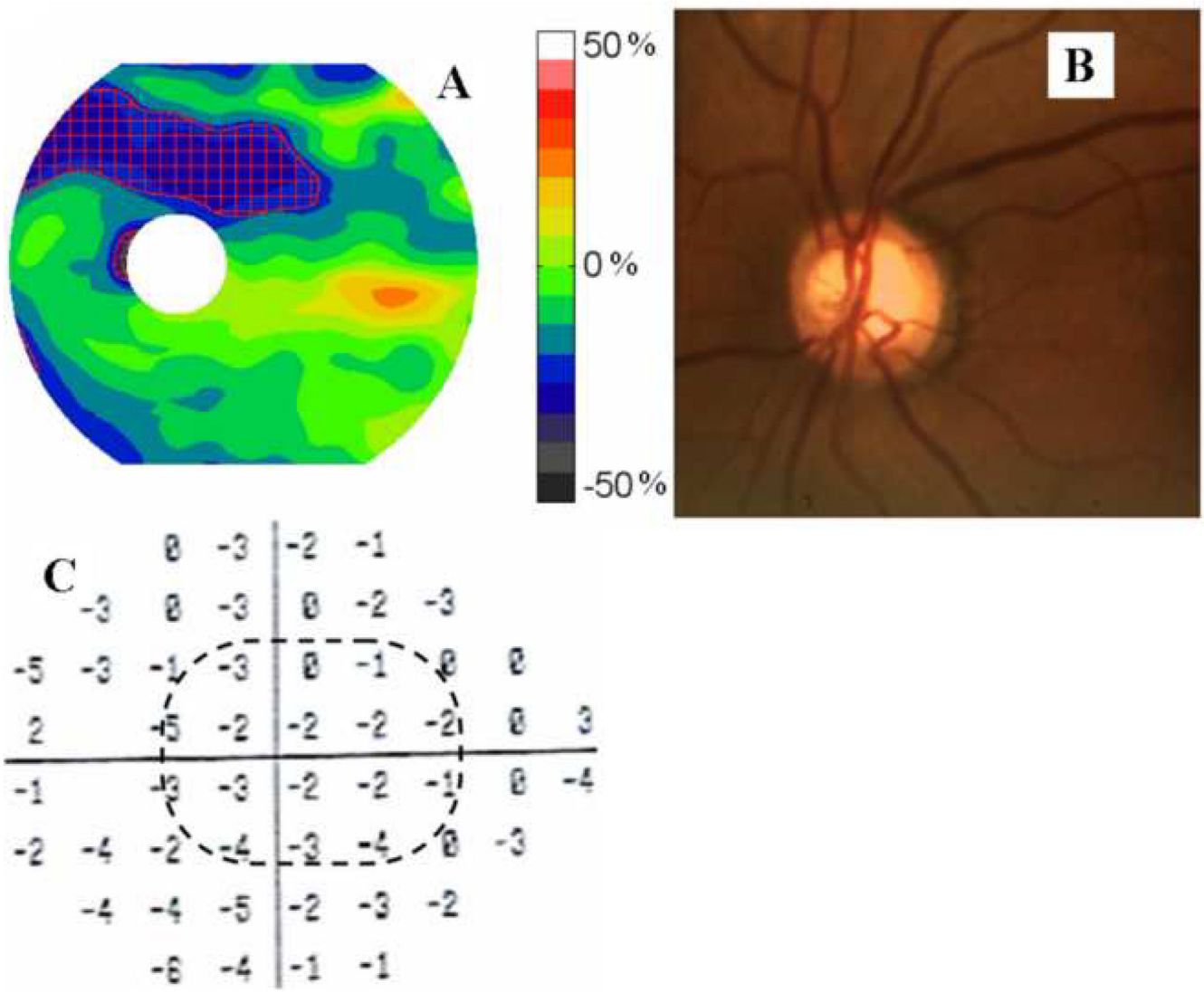

Figure 6.

A pre-perimetric glaucoma (PPG) case example. (A) Ganglion cell complex (GCC) fraction deviation (FD) map. Some of the GCC parameters were abnormal (average = 82.5 μm, p > 5%; focal loss volume (FLV) = 4.9%, P<0.5%, global loss volume (GLV) = 13.2%, p < 0.5%; pattern coefficient of variation (PCV) = 13%, P>5%; superior-inferior difference (SID) = −12.1 μm, p <0.5%;) (B) Disc photograph showed mild thinning of the superotemporal rim. (C) Visual field pattern deviation map showed scattered shallow depressions that were within the range of normal variation.

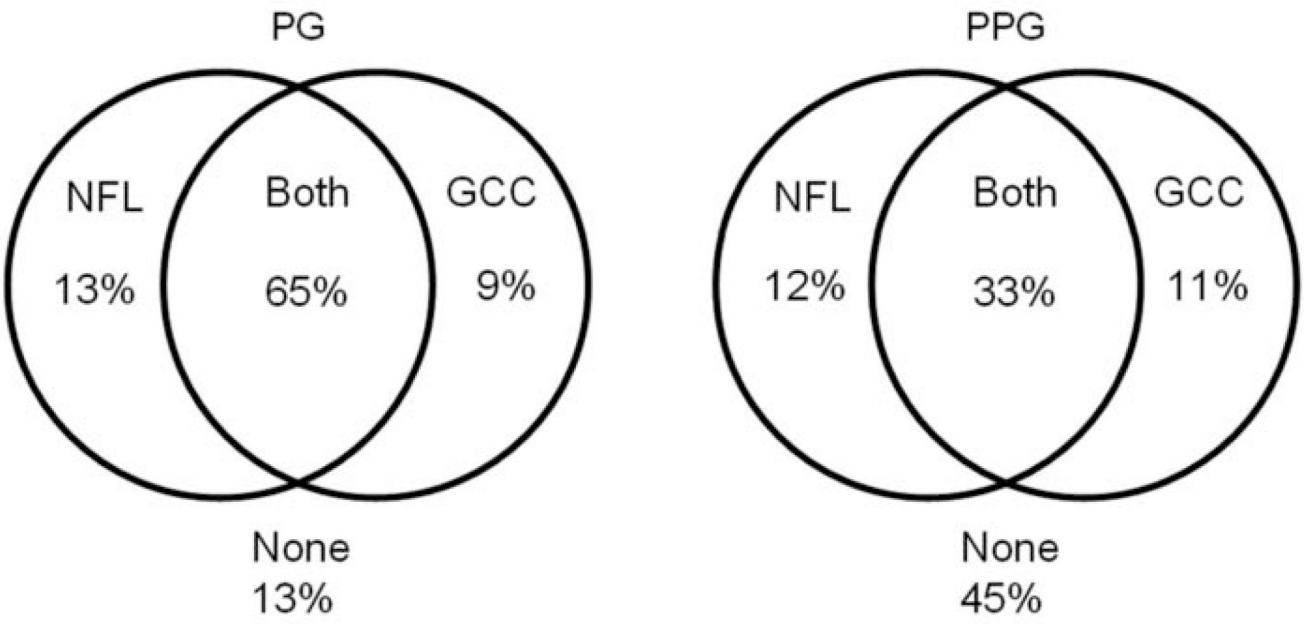

Figure 7.
Venn diagrams showing the overlap between abnormal nerve fiber layer (NFL) and ganglion cell complex (GCC) thicknesses in both perimetric glaucoma (PG) and pre-perimetric glaucoma (PPG) groups. Abnormalities were detected at the 5 percentile level.

Table 1

Characteristics of the Study Population

Group	**N**	**PPG**	***P****	**PG**	***P****
# of Participants***	65	52	-	78	-
# of Eyes	125	76	-	109	-
Age (year)****	52.9 ±8.9	60.4±9.7	<0.0001	60.5±8.4	<0.0001
Female (% total)	68%	56%	0.2	56%	0.2
Race %Caucasian	88%	79%	0.2	73%	0.03
MD (dB)****	−0.1±1.0	−0.5±1.4	0.01	−4.6±4.4	<0.0001
PSD (dB)****	1.5±0.2	1.9±1.0	0.001	6.0±4.4	<0.0001
IOP (mmHG)****	14.7±2.5	16.4±3.3	0.004	15.2±3.5	0.3
CCT (μm)****	561.3±36.8	560.0±32.4	0.7	541.9±35.8	0.007

Abbreviations: N = normal; PPG = pre-perimetric glaucoma; PG = perimetric glaucoma; MD = mean deviation (visual field); PSD = pattern standard deviation (visual field); IOP = intraocular pressure; CCT = central comeal thickness.

*P** P values for comparing N and PPG groups

*P*** P values for comparing N and PG groups

*** Some participants have one eye diagnosed as PPG and the other eye diagnosed as PG.

**** Mean±standard deviation

Table 2

The Distribution of Diagnostic Parameters by Group

Diagnostic Parameter	N		PPG		PG	
	Mean (SD)	Range	Mean (SD)	Range	Mean (SD)	Range
RTVue FD-OCT						
GCC-AVG (μm)	94.8 (7.5)	76.6,119.8	87.0 (9.3)	68.6,114.6	79.4 (10.4)	53.6,99.1
GCC-FLV (%)	−0.7 (1.9)	−17.0, 0.0001	−2.3 (2.7)	−12.5, 0.0001	−6.4 (4.3)	−14.5, 0.0001
GCC-GLV (%)	−4.3 (4.3)	−21.1, 0.001	−10.2 (7.0)	−26.6, −0.1	−17.5 (9.7)	−42.1, −1.0
GCC-PCV	0.076 (0.036)	0.041, 0.360	0.090 (0.034)	0.051, 0.240	0.133 (0.046)	0.051, 0.227
GCC-SID (μm)	3.4 (2.9)	0.02,15.8	4.2 (4.0)	0.1, 21.5	7.2 (6.0)	0.1, 24.9
MR-AVG (μm)	228.5 (13.2)	203.1, 261.6	218.9 (12.1)	194.9, 252.3	212.1 (12.4)	180.9, 237.0
Stratus TD-OCT						
NFL-AVG (μm)	98.9 (8.3)	79.5,131.4	87.7 (13.1)	60.2,114.4	77.5 (14.8)	43.5,127.5
MR-AVG (μm)	238.3 (13.0)	208.0, 264.2	229.1(14.5)	205.3, 269.7	221.7 (14.6)	180.0, 252.5

Abbreviations: N = normal; PPG = pre-perimetric glaucoma; PG = perimetric glaucoma; SD = Standard deviation; GCC = ganglion cell complex thickness; AVG = average; FLV (%) = focal loss volume expressed as a percentage of the average GCC volume in the normal group; GLV = global loss volume; PCV = pattern coefficient of variation; SID = superior - inferior difference; MR = macular retina thickness; NFL = nerve fiber layer thickness. FD-OCT: Fourier-domain optical coherence tomography; TD-OCT: time-domain optical coherence tomography

Table 3

Repeatability of Diagnostic Parameters

	N			PPG			PG		
Diagnostic Parameters	**ICC**	**SD**	**CV**	**ICC**	**SD**	**CV**	**ICC**	**SD**	**CV**
RTVue FD-OCT									
GCC-AVG (μm)	0.98	1.03	1.09	0.99	1.06	1.23	0.99	0.98	1.25
GCC-FLV (%)	0.91	0.38		0.96	0.59		0.95	1.01	
GCC-GLV (%)	0.98	0.68		0.99	0.90		0.99	1.01	
GCC-PCV	0.85	0.01		0.92	0.01		0.93	0.01	
GCC-SID (μm)	0.94	1.12		0.95	1.24		0.97	1.61	
MR-AVG (μm)	0.99	1.20	0.52	0.99	1.06	0.49	0.99	1.36	0.65
Stratus TD-OCT									
NFL-AVG (μm)	0.96	1.71	1.72	0.99	1.52	1.75	0.98	2.22	2.86
MR-AVG (μm)	0.97	2.17	0.91	0.93	3.69	1.61	0.96	3.01	1.36

Abbreviations: N = normal; PPG = pre-perimetric glaucoma; PG = perimetric glaucoma; ICC = intraclass correlation; SD: Pooled standard deviation; CV = coefficient of variation. GCC = ganglion cell complex thickness; AVG = average; FLV (%) = focal loss volume expressed as a percentage of the average GCC volume in the normal group; GLV = global loss volume; PCV = pattern coefficient of variation; SID = superior - inferior difference; MR = macular retina thickness; NFL = nerve fiber layer thickness. FD-OCT: Fourier-domain optical coherence tomography; TD-OCT: time-domain optical coherence tomography

Table 4

Diagnostic Accuracy of Diagnostic Parameters

Diagnostic Parameter	PG AROC (SE)	PPG AROC (SE)
RTVue FD-OCT		
GCC-AVG (μm)	0.90 (0.02)	0.78 (0.05)
GCC-FLV (%)	0.92 (0.02)	0.73 (0.05)
GCC-GLV (%)	0.92 (0.02)	0.79 (0.04)
GCC-PCV	0.90 (0.02)	0.72 (0.05)
GCC-SID (μm)	0.80 (0.03)	-*
MR-AVG (μm)	0.85 (0.03)	0.76 (0.05)
Stratus TD-OCT		
NFL-AVG (μm)	0.92 (0.02)	0.08 (0.05)
MR-AVG (μm)	0.85 (0.03)	0.76 (0.05)

The accuracy of diagnosing PG and PPG against the reference normal group was assessed by the area under the receiver operating curve.

Abbreviation: PPG = pre-perimetric glaucoma; PG = perimetric glaucoma; AROC= area under the receiver operating curve; SE = standard error. GCC = ganglion cell complex thickness; AVG = average; FLV (%) = focal loss volume expressed as a percentage of the average GCC volume in the normal group; GLV = global loss volume; PCV = pattern coefficient of variation; SID = superior - inferior difference; MR = macular retina thickness; NFL = nerve fiber layer thickness; FD-OCT: Fourier-domain optical coherence tomography; TD-OCT: time-domain optical coherence tomography

* The AROC was not significantly better than 0.5 and was omitted.

Table 5

Sensitivity and Specificity of Diagnostic Parameters

Threshold	5th percentile			1st percentile		
parameter	Sensitivity (PG)	Sensitivity (PPG)	Specificity	Sensitivity (PG)	Sensitivity (PPG)	Specificity
RTVue FD-OCT						
GCC-AVG	0.61 (0.05)	0.34 (0.06)	0.95 (0.02)	0.43 (0.05)	0.13 (0.04)	0.99 (0.01)
GCC-FLV	0.72 (0.05)	0.30 (0.05)	0.95 (0.02)	0.36 (0.05)	0.04 (0.03)	0.99 (0.01)
GCC-GLV	0.63 (0.06)	0.33 (0.06)	0.95 (0.02)	0.46 (0.05)	0.11 (0.03)	0.98 (0.01)
GCC-PCV	0.6 (0.05)	0.17 (0.05)	0.97 (0.02)	0.41 (0.05)	0.05 (0.03)	0.98 (0.01)
GCC-SID	0.28 (0.04)	0.09 (0.04)	0.94 (0.02)	0.16 (0.04)	0.94 (0.02)	0.99 (0.01)
MR-AVG	0.36 (0.05)	0.2 (0.06)	0.97 (0.02)	0.14 (0.04)	0.01 (0.01)	1 (0)
Stratus TD-OCT						
NFL-AVG	0.75 (0.04)	0.39 (0.06)	0.97 (0.02)	0.6 (0.05)	0.3 (0.06)	0.98 (0.02)
MR-AVG	0.37 (0.05)	0.26 (0.06)	0.97 (0.02)	0.21 (0.05)	0.05 (0.03)	0.99 (0.01)

Abbreviation: PPG = pre-perimetric glaucoma; PG = perimetric glaucoma; GCC = ganglion ceil complex thickness; AVG = average; FLV (%) = focal loss volume expressed as a percentage of the average GCC volume in the normal group; GLV = global loss volume; PCV = pattern coefficient of variation; SID = superior - inferior difference; MR = macular retina thickness; NFL = nerve fiber layer thickness; FD-OCT: Fourier-domain optical coherence tomography; TD-OCT: time-domain optical coherence tomography